Keratin 1 maintains skin integrity and participates in an inflammatory network in skin via interleukin-18

Roth, Wera ; Kumar, Vinod ; Beer, Hans-Dietmar ; Richter, Miriam ; Wohlenberg, Claudia ; Reuter, Ursula ; Thiering, Sören ; Staratschek-Jox, Andrea ; Hofmann, Andrea ; Kreusch, Fatima ; Schultze, Joachim L ; Vogl, Thomas ; Roth, Johannes ; Reichelt, Julia ; Hausser, Ingrid ; Magin, Thomas M

DOI: https://doi.org/10.1242/jcs.116574

via

[1]Translational Centre for Regenerative Medicine (TRM) and Institute of Biology, University of Leipzig, D-04103 Leipzig, Germany. [2]University Hospital, Department of Dermatology, University of Zurich, CH-8006 Zurich, Switzerland. [3]Institute of Biochemistry and Molecular Biology, Division of Cell Biochemistry, University of Bonn, D-53115 Bonn, Germany. [4]Department of Genomics and Immunoregulation, LIMES Institute, University of Bonn, D-53115 Bonn, Germany. [5]Institute of Immunology, University of MŸnster, D-48149 MŸnster, Germany. [6]Institute of Cellular Medicine and North East England Stem Cell Institute, Newcastle University, Newcastle upon Tyne NE2 4HH, UK. [7]UniversitŠts-Hautklinik, Ruprecht-Karls-UniversitŠt Heidelberg, D-69120 Heidelberg, Germany.

Krt1 controls an inflammatory network in skin

Thomas M. Magin, Translational Centre for Regenerative Medicine (TRM) and Institute of Biology, Div. of Cell and Developmental Biology, University of Leipzig, Talstrasse 33, D-04103 Leipzig, Germany, phone 0049 (0)341 97 39582, Fax 0049(0)341 97 39589, thomas.magin@trm.uni-leipzig.de*.

JCS online publication date 6 December 2012

Keratin 1 (KRT1) and its heterodimer partner keratin 10 (KRT10) are major constituents of the intermediate filament cytoskeleton in suprabasal epidermis. KRT1 mutations cause epidermolytic ichthyosis in humans, characterized by loss of barrier integrity and recurrent erythema. In search of the largely unknown pathomechanisms and the role of keratins in barrier formation and inflammation control, we show here that Krt1 is crucial for maintenance of skin integrity and participates in an inflammatory network in murine keratinocytes. Absence of Krt1 caused a prenatal increase in interleukin-18 (IL-18) and S100A8/A9, accompanied by a barrier defect and perinatal lethality. Depletion of IL-18 partially rescued $Krt1^{-/-}$ mice. IL-18 release was keratinocyte-autonomous, KRT1- and caspase-1-dependent, supporting an upstream role of KRT1 in the pathology. Finally, transcriptome profiling revealed a Krt1-mediated gene expression signature similar to atopic eczema (AE) and psoriasis, but different from Krt5-deficiency and epidermolysis bullosa simplex (EBS). Our data suggest a functional link between KRT1 and human inflammatory skin diseases.

157 words

Keratin cytoskeleton, epidermal barrier, innate immunity, interleukin-18, atopic eczema

The epidermis protects an organism against mechanical injury, dehydration and regulates immune homeostasis by virtue of epidermal keratinocytes (Simpson et al., 2011). Many of their functions depend on structural proteins including keratins (Kim and Coulombe, 2007; Magin et al., 2007). Keratins constitute the intermediate filament (IF) cytoskeleton in all epithelia (Schweizer et al., 2006). The type II keratin KRT1 and its heterodimer type I partner KRT10 form the major cytoskeleton in suprabasal keratinocytes. Their upregulation precedes expression of filaggrin and cornified envelope proteins. Covalent crosslinking of Krt1 but not Krt10 to these proteins, in addition to a complex series of lipids, ultimately forms the cornified/lipid envelope, that constitutes the epidermal barrier together with Langerhans cells (Candi et al., 2005; Simpson et al., 2011). This led to the hypothesis that a subset of keratins and the associated protein filaggrin are crucial for barrier function. In fact, KRT1 and KRT10 mutations lead to congenital epidermolytic ichthyosis (EI, MIM 113800) characterized by skin erosions, hyperkeratosis and barrier defects (Arin et al., 2011; Lane and McLean, 2004; Schmuth et al., 2001; Segre, 2006), whereas mutations in filaggrin can cause the inflammatory disorder atopic eczema (AE) (Brown and McLean, 2012; Oji et al., 2010). EI is characterized by skin erosions, hyperkeratosis and barrier defects (Lane and McLean, 2004; Schmuth et al., 2001; Segre, 2006). While these disorders have established a primary role of keratinocyte-resident proteins in acute and chronic skin diseases (Brown and McLean, 2012; Nestle et al., 2009; Quigley et al., 2009), the underlying pathomechanisms remain not well understood.

Besides professional immune cells, keratinocytes regulate skin inflammatory and immune responses by secretion of cytokines, antimicrobial peptides and by expression of MHCII proteins (Nestle et al., 2009). S100A8 and A9 proteins belong to the S100 family of calcium-binding proteins which can act as antimicrobial peptides and are released upon barrier defects by unconventional secretion as heterodimers. Once released, they act as autocrine activators of Toll-like receptor (TLR) 4 on keratinocytes (Eckert et al., 2004; Ehrchen et al., 2009; Nestle et al., 2009; Vogl et al., 2007). They are elevated in psoriatic skin and therefore are linked to inflammatory skin diseases (Nestle et al., 2009). Interleukins (IL) IL-18 and IL-33 are pro-inflammatory cytokines of the IL-1 family produced by suprabasal keratinocytes (Dinarello, 2009). Skin-specific overexpression of IL-18 in mice results in AE-like inflammatory lesions

(Konishi et al., 2002), and IL-18 levels are elevated in humans suffering from AE (Kou et al., 2012). IL-18 is synthesized with an amino-terminal propeptide requiring cleavage by caspase-1 or other proteases before unconventional secretion from cells, including keratinocytes (Dinarello, 2009). Activation of caspase-1 is tightly regulated by the inflammasome, a large cytoplasmic multiprotein complex consisting of scaffold proteins like NLRP3 in keratinocytes, the adaptor protein ASC (apoptosis-associated speck-like protein containing a caspase recruitment domain) and procaspase-1/-5 (Davis et al., 2011). The mechanisms controlling inflammasome activation are partially understood and include TLRs, sensing either pathogen-associated molecular patterns (PAMPs) or NOD and RIG receptors, recognizing self-derived danger signals, including nucleic acids, ATP, cholesterol crystals and amyloid beta(Davis et al., 2011). An intriguing question is whether the keratinocyte cytoskeleton is involved in intracellular damage control.

To test this hypothesis, we have generated *Krt1*$^{-/-}$ mice. In contrast to Krt10 deficiency which led to viable mice with a mild phenotype (Reichelt et al., 2001), loss of Krt1 caused perinatal lethality and a barrier defect. Transcriptional profiling revealed a gene expression signature in *Krt1*$^{-/-}$ skin similar to the human inflammatory skin diseases AE and psoriasis. Depletion of IL-18 partially rescued *Krt1*$^{-/-}$mice. Our data identify keratin proteins as gatekeepers of immune responses in skin and link cytokine release to the loss of KRT1.

!"

#"

$" K

%" To address isotype-specific keratin functions during epidermal differentiation and barrier

&" formation (Kim and Coulombe, 2007; Magin et al., 2007) we generated Krt1-deficient mice (

'" , ;). Surprisingly, the absence of Krt1 caused neonatal

(" lethality in a mixed 129/Ola x C57BL/6 genetic background, unlike Krt10 depletion (Reichelt et

)" al., 2001). Histology of neonatal *Krt1*$^{Đ/Đ}$ skin revealed a largely intact stratified epidermis,

*" without local inflammation and localized keratinocyte lesions, possibly upon handling-induced

!+" trauma. Further, the granular layer was reduced ( ). Expression of Krt10, the obligate

!!" heterodimer protein partner of Krt1, was significantly reduced in *Krt1*$^{-/-}$ skin extracts, but its

!#" intracellular distribution remained unaltered (,). Electron microscopy revealed sparse

!$" keratin aggregates in *Krt1*$^{-/-}$ skin due to loss of Krt1, indicating lack of compensatory keratins,

!%" and normal filaments in wild-type epidermis ( ). Krt5 and

!&" Krt14, typically restricted to basal keratinocytes, were present in suprabasal *Krt1*$^{Đ/Đ}$ skin, and

!'" their protein level was slightly elevated, similar to other epidermis-specific knockouts

!(" ( ).In *Krt10*$^{-/-}$ mice, no Krt1 aggregates were detectable, but

!)" atypical IF between Krt1 and Krt14 were present and contributed to skin integrity (Reichelt et

!*" al., 2001). To address whether Krt10 assembled with type II keratins Krt5 or Krt6 in *Krt1*$^{-/-}$

#+" epidermis, high resolution confocal imaging was performed. This revealed presence of numerous

#!" Krt10 aggregates without Krt5 or Krt6 in spinous layer keratinocytes, indicating that upon

##" expression of Krt10, no type II partner is available to form intermediate filaments (Fig. 2A-B). In

#$" the absence of Krt1, the distribution and staining intensity of major desmosomal proteins

#%" desmoplakin, desmoglein1 and 2 and plakoglobin were unaffected (Fig. 2C-E).This suggested

#&" that both presence and intracellular organization of Krt5/14 filaments in suprabasal epidermis

#'" maintained desmosome functionality.Distribution and expression levels of cornified envelope

#(" (CE) proteins loricrin, involucrin and filaggrin (;

#)" and data not shown) appeared unaltered, supporting occurrence of terminal differentiation. A

#*" strong hint on disturbed skin homeostasis came from the appearance of stress-associated Krt6

$+" and Krt16 induced upon hyperproliferation, barrier defects and wound healing (Kim and

Coulombe, 2007)(;). The mild skin defects of *Krt1*$^{-/-}$ and the notion that *Krt1*$^{-/-}$, in contrast to *Krt10*$^{-/-}$ mice, are not viable (Reichelt et al., 2001; Reichelt and Magin, 2002), point towards a novel and unique function of Krt1 *in vivo*. This is also in agreement with the recently described phenotype of Krt1/10 doubly-deficient mice (Wallace et al., 2012).

The known participation of KRT1, but not KRT10 to cornified envelope formation (Candi et al., 2005; Candi et al., 1998) and a mild weight loss of *Krt1*$^{D/D}$that manifested postnatally ( ) prompted us to examine epidermal barrier integrity employing an established dye-penetration assay (Segre et al., 1999).This established an intact outside-in epidermal barrier in *Krt1*$^{-/-}$ newborns, as no dye penetrated the skin ( ). In contrast, trans-epidermal water loss (TEWL) was increased twofold in neonatal*Krt1*$^{-/-}$ mice, revealing a defective inside-out barrier ( ).Possibly, the biotin assay performed in Krt1/10-doubly-deficient mice may not fully reveal the barrier state of these mice (Wallace et al., 2012). Further, the number of intact cornified envelopes was significantly reduced to ~17% in *Krt1*$^{-/-}$ compared to ~84% in *Krt1*$^{+/+}$ and ~55% in *Krt10*$^{+/+}$mouse skin (, and ;).Together with the notion that in Krt1/10 doubly-deficient mice 60 % of cornified envelopes remained intact (Wallace et al., 2012), our data substantiated a

downregulated in *Krt1*$^{Đ/Đ}$ mice. Gene set enrichment analysis, followed by gene ontology classification and grouping according to function (Keller et al., 2008) of genes upregulated in *Krt1*$^{Đ/Đ}$ skin, revealed a similar distribution of function categories in E18.5 and newborn samples (,). Strikingly, cluster analysis and heat maps identified a significant over-representation of genes linked to CE formation/epidermal differentiation (,) and inflammatory/immune defense pathways (,) in E18.5 and newborn *Krt1*$^{Đ/Đ}$ skin, demonstrating that both gene sets were altered prenatally. To validate array data, selected candidate gene expression was confirmed by quantitative RT-PCR ( ). Prenatal upregulation of pro-inflammatory genes strongly supported a direct involvement of Krt1 in the regulation of the above pathways. The pattern of genes upregulated in *Krt1*$^{Đ/Đ}$ skin, e.g. Il-1β, IL-18, defensins and S100 proteins, bore resemblance with the human inflammatory skin diseases atopic eczemia (AE) and psoriasis, characterized by barrier defects, inflammation and immune dysregulation (Barnes, 2010; Gudjonsson et al., 2010; Gudjonsson et al., 2009; Saaf et al., 2008; Suarez-Farinas et al., 2010; Suarez-Farinas et al., 2011). We then focused on IL-18, as cytokine analysis of E18.5 serum samples confirmed its elevation (see below, Fig. 5A). To substantiate this further, global comparisons between the *Krt1* data set (our study) and genome-wide transcriptional profiling data sets derived from AE and psoriasis patients were performed (Gudjonsson et al., 2010; Saaf et al., 2008).The intersection of similarly regulated genes between *Krt1*$^{Đ/Đ}$ skin versus AE or psoriatic skin was remarkably high, with 55 (E18.5) and 154 (P0) genes compared to AE skin, and 86 (E18.5) or 166 genes (P0) compared to psoriatic skin (; and). Genes similarly regulated between *Krt1*$^{Đ/Đ}$ and AE skin comprise IL-18, S100A8/A9, Il6/Il6R, SOCS3, KLK, TGM and SPRR (and), genes described to be associated with AE (Barnes, 2010; Saaf et al., 2008; Suarez-Farinas et al., 2011). In analogy, genes upregulated in *Krt1*$^{Đ/Đ}$ and psoriatic skin were compared. This uncovered a group of genes previously ascribed to psoriasis, including epidermal barrier-coding genes, e.g. SPRRs, S100, KLKs, IL-1 family members and genes of lipid metabolism (ELOV and fatty acid binding protein, FABP) (Gudjonsson et al., 2010; Gudjonsson et al., 2009; Suarez-Farinas et al., 2010) (and). In striking contrast, the comparison of genes upregulated in *Krt1*$^{Đ/Đ}$ versus *Krt5*$^{Đ/Đ}$ mouse skin which serve as a model for the keratin-associated disease epidermolysis bullosa simplex (EBS) was very low, with 14 genes for E18.5 and 23 genes for P0

!" *Krt1*$^{Đ/Đ}$ skin(Lu et al., 2007) ( ). Furthermore, only 11 upregulated genes at E18.5 and 18
#" genes at P0 *Krt1*$^{Đ/Đ}$ skin were common to human EBS patient skin (Bchetnia et al., 2012). Based
$" on these data we conclude that the gene expression signature from *Krt1*$^{Đ/Đ}$ mice shows more
%" similarities to human inflammatory skin diseases than to keratin-associated defects in mice and
&" humans ( ).
'" To further dissect the role of Krt1 in inflammation, gene set enrichment analysis (GSEA) was
(" performed to identify commonly regulated pathways in *Krt1*$^{Đ/Đ}$versus AE and*Krt1*$^{Đ/Đ}$versus
)" psoriatic skin. Remarkably, the pathway network obtained for the *Krt1*$^{Đ/Đ}$ versus AE intersection
*" (; and) showed a striking similarity to the AE
!+" pathway. Resulting data were compared to an Ingenuity Pathway Analysis based on 81 validated
!!" AE genes (Barnes, 2010), which detects expression patterns of genes whose expression is linked
!#" to distinct signaling pathways. This highlighted the functional significance of IL-1 family
!$" members such as IL-18, TLR/MYD88 signaling, and NOD-like receptor family members (NLR)
!%" in Krt1$^{Đ/Đ}$mice and in AE. In contrast, the pathway network obtained for the *Krt1*$^{Đ/Đ}$versus
!&" psoriasis intersection was less extended and showed a limited interconnection of functional
!'" clusters (data not shown). These data suggested a link between Krt1 and IL-18.
!("
!)"
!*" To further substantiate Krt1 involvement in an inflammatory network in keratinocytes, we
#+" focused on IL-18 and related pro-inflammatory cytokines. Quantitative RT-PCR showed a
#!" significant upregulation of IL-18in E18.5 *Krt1*$^{Đ/Đ}$ skin ( ),
##" consistent with its marked elevation at the protein level in suprabasal, neonatal *Krt1*$^{Đ/Đ}$ skin and
#$" in the dermis ( ). Moreover, IL-18 levels were significantly elevated in the serum of
#%" newborn *Krt1*$^{Đ/Đ}$ mice ( ). In line with the AE-like phenotype resulting from ectopic
#&" expression of IL-18 in mouse epidermis and the recent identification of high serum IL-18 in AE
#'" patients (Kambe et al., 2010; Konishi et al., 2002; Kou et al., 2012), our data support a role of
#(" IL-18 in the pathology of *Krt1*$^{Đ/Đ}$ mice. Further, the levels of IL-33, another member of the IL-1
#)" family, were markedly increased in epidermal extracts of *Krt1*$^{Đ/Đ}$ mice, but only mildly increased
#*" in newborn *Krt1*$^{Đ/Đ}$ serum ( ). IL-33 is known to be expressed in the suprabasal epidermis
$+" and the lung where it mediates a pro-inflammatory response by activating mast cells and Th2
$!" lymphocytes. Its upregulation has been associated to allergic airway diseases and asthma

(Haraldsen et al., 2009). The antimicrobial peptides S100A8 and S100A9, two damage-associated molecular pattern (DAMP) molecules linked to compromised skin barrier function and inflammatory skin diseases (Ehrchen et al., 2009), were strongly induced in suprabasal *Krt1*$^{Þ/Þ}$ epidermis, where Krt1 is normally expressed, but also in the dermis, supporting an inflammatory response (,). Moreover, thymic stromal lymphopoietin (TSLP), a cytokine produced by differentiated keratinocytes (Ziegler and Artis, 2010), was increased in *Krt1*$^{Þ/Þ}$ epidermal extracts ( ). TSLP has been implicated in atopic dermatitis and is a master switch for allergic inflammatory airway diseases in mice (Ziegler and Artis, 2010). The elevated expression of these cytokines in *Krt1*$^{Þ/Þ}$ mice and in AE (Ehrchen et al., 2009; Suarez-Farinas et al., 2011) lends further support to a role of Krt1 in controlling skin inflammation.

Next, we examined whether elevated cytokine levels might be connected to erythema and to additional systemic defects noted in epidermolytic ichthyosis (Arin et al., 2011). Staining for platelet endothelial cell adhesion molecule (PECAM) was increased, indicating increased vascularization at the dermal/epidermal interface (; ,). In line with these findings, lungs from P0 *Krt1*$^{Þ/Þ}$ pups had higher blood cell numbers (,) and displayed capillary leakage ( ). Finally, the expression of the prominent pro-inflammatory cytokines IL-1α and TNFα remained unaltered in *Krt1*$^{Þ/Þ}$ mice (data not shown), underscoring the selectivity of Krt1ûs function.

To validate our hypothesis that KRT1 restrains inflammation and an innate response in the epidermis by promoting barrier acquisition and restricting IL-18 release, we decided on a rescue of *Krt1*$^{Þ/Þ}$ mice following antibody-mediated depletion and loss-of-function approaches. Surprisingly, systemic administration of IL-18-blocking antibodies to pregnant females extended the lifespan of *Krt1*$^{Þ/Þ}$ pups for at least 2 days. The antibody-mediated IL-18 blockade (;) increased the percentage of intact CEs (~32% versus ~15% in isotype-treated controls), indicating a crucial role of IL-18. To gather additional evidence, a genetic rescue experiment was conducted, crossing *Krt1*$^{Þ/Þ}$to *Il18*$^{-/-}$- knockout mice (Hochholzer et al., 2000). Double heterozygous *Krt1*$^{+/Þ}$*Il18*$^{+/Þ}$ mice were interbred and offspring

that survived until 4-6 weeks of age was assessed for homozygotes. Loss of IL-18 resulted in a partial rescue of *Krt1*$^{Đ/Đ}$ mice, since 12 *Krt1*$^{Đ/Đ}$*Il18*$^{Đ/Đ}$survivors were obtained from 16 expected survivors (75%), compared to only 6 *Krt1*$^{Đ/Đ}$*Il18*$^{+/+}$expected from 16 survivors (37.5%) in a *Il18* wild-type genetic background ( ). In contrast, the equivalent rescue experiment using a S100A9-deficient background (Manitz et al., 2003) generated no survivors (data not shown). Rescued *Krt1*$^{Đ/Đ}$*Il18*$^{Đ/Đ}$double-deficient mice displayed an apparently normal epidermal morphology similar to*Krt1*$^{Đ/Đ}$mice (, ; ,). Analysis of cornified envelopes revealed a twofold increase in intact CEs from newborn *Krt1*$^{Đ/Đ}$*Il18*$^{Đ/Đ}$ skin compared to corresponding *Krt1*$^{Đ/Đ}$skin at P0, in line with the results obtained by the antibody blocking experiment (, ;). Thus, we conclude that Krt1 acts upstream of IL18.

Having established a major role of IL-18 in Krt1 pathology, we sought to identify the underlying mechanism responsible for its release from keratinocytes. Engagement of intracellular NOD-like receptors (NLRs) by pathogen- or danger-associated molecular pattern molecules activates inflammasomes and caspase-1 which cleaves IL-18 into its active form (Davis et al., 2011; Schroder and Tschopp, 2010; Strowig et al., 2012).Remarkably, NLRP3 (nucleotide-binding-domain, leucine-rich repeat containing protein) was localized in a keratin-dependent manner in mouse keratinocytes. In contrast to control keratinocytes, NLPR3 distribution appeared more diffuse in keratinocytes in which we had depleted the entire keratin family (Seltmann et al., 2012; Vijayaraj et al., 2009), suggesting a contribution of keratins to the regulation of inflammasome activity ( ). We analyzed whether IL-18 processing occurs in a KRT1-dependent manner in human keratinocytes which are known to express higher amounts of KRT1 compared to murine cells upon differentiation (Feldmeyer et al., 2010). Unstimulated human keratinocytes produce significant amounts of proIL-18 but don̂t release mature IL-18 ( ). Upon UVB irradiation, known to increase inflammasome activity and IL-1β release from keratinocytes (Feldmeyer et al., 2007), mature IL-18 was released into the supernatant. Using two caspase-1 inhibitors, IL-18 release could be blocked ( ). This demonstrated functionality of the cell system. A knockdown of KRT1 in differentiated human primary keratinocytes resulted in secretion of cleaved IL-18, whereas a simultaneous knockdown of

caspase-1 blocked the release of this cytokine ( ). This highlighted an important role of KRT1 in inflammasome activation. Thus, Krt1, in contrast to its heterodimer partner Krt10, has unique functions in the maintenance of the cornified envelope,barrier formation and in restraining IL-18 release from keratinocytes. Both Krt1 and Krt10 share an important function in the maintenance of epidermal integrity (Fig. 8; (Wallace et al., 2012).

The epidermal barrier is formed by keratinocytes contributing tight junctions and the cornified envelope and by Langerhans cells providing immune functions (Simpson et al., 2011). Barrier dysfunction and cutaneous sensitization can give rise to chronic inflammatory disorders including atopic eczema (AE) and psoriasis. While both cell types are crucial for barrier functionality, the significance of epithelial keratinocytes in acute and chronic immune disorders has been disputed for long. The recent discovery of filaggrin mutations as an underlying cause of AE has highlighted a major role of keratinocytes in shaping immune responses, following barrier disruption and secretion of cytokines including IL-18, IL-33 and TSLP (Haraldsen et al., 2009; Wittmann et al., 2009; Ziegler and Artis, 2010). These seminal findings raise the issue whether additional keratinocyte-resident proteins contribute to barrier defects and immune disorders through analogous mechanisms.

Until recently, keratins were predominantly regarded as intracellular scaffolds protecting epithelia against mechanical insults, in apparent agreement with phenotypes observed in epidermal keratinopathies (Arin et al., 2010; Arin et al., 2011; Chamcheu et al., 2011; Kim and Coulombe, 2007; Magin et al., 2007). Here, we show for the first time that Krt1, a member of the keratin family of cytoskeleton proteins, plays a major role in epidermal barrier formation and in restricting IL-18 release from keratinocytes, in addition to its role in preserving cell integrity upon elevated mechanical stress. Most importantly, cornified envelope defects, transcriptional upregulation and release of distinct cytokines manifest prenatally upon loss of Krt1, underlining its primary involvement. The specificity of Krt1 is further supported by the very mild phenotype of mice lacking Krt10, its heterodimer partner (Reichelt et al., 2001). As one might predict, combined deletion of *Krt1/10* was accompanied by skin fragility more severe than in single gene knockouts (Wallace et al., 2012). In the absence of a side-by side analysis of both mice we speculate that the apparently more severe phenotype of *Krt1/10*$^{-/-}$ compared to *Krt1*$^{-/-}$ is connected to the presence of cytoplasmic Krt10 aggregates in the latter. The limited extent of cell fragility in all three mouse models and the notion that Krt1, but not Krt10, is covalently cross-linked to the CE (Candi et al., 1998) together with or data underscore unique Krt1 functions (see also Fig. 8).

The prenatal upregulation of IL-18 that occurred at transcriptional and posttranscriptional levels, together with data showing KRT1- and caspase-1-dependent IL-18 release from cultured keratinocytes place Krt1 upstream of IL-18. The importance of IL-18 in this setting is underscored by the partial pharmacological and genetic rescue of the Krt1 phenotype. Collectively, these data suggest a link between components of the epithelial cytoskeleton and inflammasome activation which might contribute to alter immune responses from a Th1 to a Th2 profile (Kou et al., 2012; Wittmann et al., 2009). In support, absence of Krt17 was reported to attenuate inflammation in models of acute dermatitis, characterized by a change in inflammatory cytokines from a Th1- and Th17- toa Th2-dominated inflammatory response(Depianto et al., 2010).Most recently, fragments of Krt6A were reported to display antimicrobial activity in corneal keratinocyte extracts(Tam et al., 2012). Given the slightly elevated fragility of Krt1/IL-$18^{-/-}$ epidermis, such an activity, if conserved in mouse epidermal keratinocytes, might contribute to the absence of strong inflammation in surviving animals.

The inflammatory signature in *Krt1*$^{Đ/Đ}$mice bears similarity to atopic eczema, linked to mutations in the keratin-associated protein filaggrin (Brown and McLean, 2012). The similarity of cytokine profiles and of commonly regulated pathways in *Krt1*$^{Đ/Đ}$ mice and AE patients raise the issue whether Krt1 acts through filaggrin-dependent mechanisms. We find that the absence of Krt1 does not affect filaggrin processing ( ). Further, elevation of pro-inflammatory cytokines in filaggrin-related AE represents a late event, possibly resulting from a defective barrier and the responding immune system (Brown and McLean, 2012; Kezic et al., 2012; Kou et al., 2012). In contrast to prediction, deletion of filaggrin in mice does neither affect survival nor cause an elevated trans-epidermal water loss, but results in enhanced responses in contact hypersensitivity (Kawasaki et al., 2012). The unexpectedly mild phenotype arising from complete loss of filaggrin leads to the question whether KRT1 is involved. In a wider context, our data raise the issue if conditions in which KRT1 is mutated, e.g. epidermolytic ichthyosis, or downregulated, e.g. squamous cell carcinoma, cutaneous wound healing and HPV infections (Arin et al., 2011; Depianto et al., 2010; Longworth and Laimins, 2004) carry an inflammatory signature similar to that seen in *Krt1*$^{Đ/Đ}$ mice. Our data connect presence of KRT1 to a keratinocyte-based network that restrains inflammation and, in conjunction with Krt17 (Depianto et al., 2010), provide strong evidence for context-dependent functions of keratin isotypes that extend beyond formation of cytoskeletal scaffolds in epithelia.

Krt1$^{Đ/Đ}$ mice were generated by targeted disruption of *Krt1* gene *via* homologous recombination in embryonic stem cells ( ). Hence, exon1, intron 1 and ~415 bp from the 5Ô UTR were deleted and replaced by an Hprt-minigene cassette (Reichelt et al., 2001). All mice were from a mixed 129/SvJxC57BL/6 background. Experiments were performed according to institutional regulations. Offspring from heterozygous intercrosses were genotyped by PCR analysis of tail DNA (for details). Genotypes of *Krt1*$^{Đ/Đ}$ offspring were confirmed by Western blot analysis of skin protein extracts with a polyclonal anti-Krt1 rabbit antiserum.

See in the Supplementary material.

Preparation of tissue samples and immunofluorescence analysis were carried out as described (Roth et al., 2009). HorseradishÐconjugated secondary antibodies were detected by the Super Sensitive Link-Label IHC Detection System (BioGenex Laboratories, Fremont, CA, USA) with diaminobenzidine (Dako, Hamburg, Germany). Images were acquired at ambient temperature with an Axioplan 2 fluorescence microscope (Carl Zeiss, Jena, Germany) equipped with Zeiss Plan-Apochromat 63x/1.4 and Plan-Neofluar 40x/1.3 oil immersion objectives, and recorded with an AxiocamHR camera (Carl Zeiss, Jena, Germany). Image analysis and processing were performed using the AxioVision 4.6 software (Carl Zeiss, Jena, Germany). Confocal images were recorded on an LSM710 microscope equipped with a Zeiss63x LCI Plan Neofluar objective (Carl Zeiss, Jena Germany). Fluorochromes were scanned in sequential scans to avoidcross-talk between channels using Pinhole ÔÔairy 1ÓZeiss standard settings. Z-stacks of 8-12 consecutive sections were recorded and processed as Ò maximum intensity projectionÓ. Image analysis and processing were performed with the Zen software (Carl Zeiss, Jena, Germany). Images were cropped and analyzed in Adobe Photoshop CS4; Adobe Illustrator CS4 was used for figure design.

Full-thickness skin samples were lysed in 5x Laemmli buffer and homogenized (Ultra Turrax). Immunoblot analysis was performed as described(Loffek et al., 2010).

Full-thickness mouse skin was floated on 0.5 M ammonium thiocyanate (Sigma-Aldrich, St. Louis, MO, USA) as described (Reichelt and Magin, 2002) to

isolate epidermal sheets.

Epidermal sheets or full-thickness skin samples were homogenized (Ultra-Turrax) in TRIzol (Life Technologies, Darmstadt, Germany) supplemented with ribonucleoside-vanadyl complexes (New England BioLabs, Ipswich, Ma, USA). Total RNA was phenol/chloroform extracted, precipitated followed by DNaseI treatment (Fermentas Life Science, Leon-Rot, Germany), and purified with the RNeasy MinElute Cleanup kit (Qiagen, Hilden, Germany).

. The MouseWG-6v2.0 Expression BeadChip kit (Illumina, Inc., San Diego, CA, USA) was used to probe triplicate *Krt1*$^{+/+}$ and *Krt1*$^{Đ/Đ}$ samples Data analysis was based on the R Statistical language (R Development Core Team 2007, 2.8.0) and the Beadstudio 3.1.1.0 software. Data were quantile-normalized. A fold-change/p-value filter was used to select differentially expressed genes; p-values smaller than 0.05, expression changes higher than 2-fold and a difference between mean intensity signals greater background were considered statistically significant. The false discovery rate (FDR) of p-values was adjusted by the Benjamini-Hochberg method. Heatmaps were generated based on average linkage and the pearson correlation coefficient. Blue indicates for low level, white for intermediate, and red for high levels of gene expression. The gene expression data sets are deposited at the GEO database (GES32951).

Transcriptome data from AE (E-GEOD-12511), psoriasis (E-GEOD-13355), *Krt5* P0 (E-GEOD-7663) and EBS (E-GEOD-28315) were downloaded from the EBI server for the further comparison analysis(Bchetnia et al., 2012; Gudjonsson et al., 2010; Lu et al., 2007; Saaf et al., 2008). For data processing GNU R (www.r-project.org) with the Bioconductor packages (www.bioconductor.org) were used. Data were normalized by RMA algorithms. *Krt1* data were individually analyzed or evaluated in conjunction with the additional transcriptome data sets.

For cross platform and a cross species comparison the transcriptome data sets (A and B) were annotated by gene symbols and normalized by its standard deviation. In the first step of this normalization the gene expression ($y_{i,j}$) of the gene (i) on array (j) in set A was normalized by the following equation:

$$y'_{i,j} = \frac{y_{i,j} - \mu_{setA}}{\sigma_{setA}} \sigma_{setA \cup B} + \mu_{setA \cup B} \qquad (1)$$

Secondly the cross species adaption was achieved by equalizing the controls of each set by the following equation:

$$y''_{i,j} = y'_{i,j} - \overline{y}'_{i,j\in controlsofsetA} + \overline{y}'_{i,j\in controlsofsetA\cup B} \qquad (2)$$

The Molecular Signatures Database (MSigDB database v3.0, Broad Institute) was used. To minimize the noise the enrichment score of each set was calculated by root square means. *P*-values were calculated by Students t test. To calculate the similarity of *Krt1* data and the additional expression data sets the minimum difference to the control was used:

$$y'''_i = \mathrm{sgn}\left(\frac{\overline{y}''_{i,A} - \overline{y}''_{i,controle}}{y''_{i,B} - \overline{y}''_{i,controle}}\right) \circ MIN\left(\left|\overline{y}''_{i,A} - \overline{y}''_{i,controle}\right|, \left|\overline{y}''_{i,B} - \overline{y}''_{i,controle}\right|\right) \qquad (3)$$

Network figures of the enriched pathways were generated by the Cytoscape tool version 2.6.1 (www.cytoscape.org) with the Enrichment Map plug in(Merico et al., 2010). The top 100 enriched pathways with a p-value < 0.001 were used.

cDNA synthesis was carried out using RevertAid H Minus First Strand cDNA Synthesis kit (Fermentas Life Science, Leon-Rot, Germany). Real-time PCR was performed with Maxima SYBR Green/ROX qPCR Master Mix (Fermentas Life Science, Leon-Rot, Germany) and run on a Mastercycler ep realplex (Eppendorf, Hamburg, Germany). 18S RNA was used as a reference. Mouse qPCR primer sequences are shown in .

IL-18 and IL-33 was measured by ELISA (Bender MedSystems, Viena, Austria; Quantikine, R&D Systems, Minneapolis, MN, USA). Mrp8-Mrp14 protein levels were determined by ELISA as described(Vogl et al., 2007). TSLP protein levels were determined by mouse cytokine antibody array analysis (C series 1000.1, RayBiotech, Inc., Norcross, GA, USA) as described (Roth et al., 2009).

TEWL was assessed in triplicate readings on the dorsal neck skin of newborn mice using a Tewameter (TM 300, Courage and Khazaka Electronic, Cologne, Germany).

. Females were injected i.p. at E18.5 with 20 µg of anti-IL-18 blocking antibody (clone 93-10C, R&D Systems, Minneapolis, MN, USA) or IgG1 immunoglobulins (R&D Systems, Minneapolis, MN, USA) as control. Newborn pups were treated with 4 µg of antibody or IgG1 at P0 and P1. At P2, mice were sacrificed and analyzed.

. In human primary keratinocytes (Feldmeyer et al., 2007), differentiation was induced by culture in KBM-2 (Cambrex, East Rutherford, NJ, USA) for 6 days. Keratinocytes were UV-irradiated with 50 mJ/cm^2 (Medisun HF-54, Schulze &Boehm, Bruehl, Germany) in the presence of YVAD (20 μM), VAD (10 μM) (Enzo Life Sciences, Lorrach, Germany) or dimethyl sulfoxide (vehicle) and harvested after 4 h.For knock-down experiments, 10 nM siRNAs and Interferin (Polyplus transfection, Illkirch, France) were used. Cells and supernatants were harvested after 6 days; total protein from the supernatant was acetone-precipitated. Sequence information of siRNAs (Sigma-Aldrich, St. Louis, MO, USA) used is provided in .

Statistical significance was determined by unpaired *t* test for two groups and analysis of variance test for more than two groups. The alpha level was set at <0.05. Data were analyzed with Sigma Plot 11.0 and plotted with Excel. All statistical data are shown in .

at http://jcs.biologists.org/lookup/suppl/doi:

We thank Roland Bornheim for the generation of the *Krt1*$^{+/-}$ mouse line. We thank B. Fuss and M. Hoch for access to their LSM710. The authors declare that no competing financial interests exist.

This work was partially supported by grants from the Thyssen Foundation (T.M.M., J.Reichelt), BONFOR, Deutsche Forschungsgemeinschaft, DFG [MA1316/9] and Translational Centre for Regenerative Medicine Leipzig [BMBF, PtJ-Bio, 0315883; T.M.M.]. The authors declare that no competing financial interests exist.

Author contributions: W.Roth conceived the study, designed and performed the experiments, analyzed data, prepared the figures, and wrote the paper. V. Kumar performed experiments and analyzed data. H.-D. Beer performed the siRNA transfections and immunoblots to study inflammasome activation. M. Richter, C.Wohlenberg and U.Reuter assisted with experiments. S. Thiering performed the bioinformatic analysis. A. Staratschek-Jox, A. Gaarz, F. Kreusch and J.L. Schultze performed the global gene expression analysis. T. Vogl and J.Roth performed Mrp-specific ELISAs and provided Mrp8/Mrp14 antibodies. J. Reichelt supervised the generation of the *Krt*$^{+/-}$ mouse line and contributed to the characterization of the initial *Krt1*$^{+/-}$ and *Krt1*$^{-/-}$ mice. I. Hausser performed the electron microscopy analysis. T.M. Magin generated *Krt1*$^{-/-}$ mice and contributed expertise, designed experiments, and wrote the paper.

!"

#"

$"

%" (2010). Identification of novel and
&" known KRT5 and KRT14 mutations in 53 patients with epidermolysis bullosa simplex: correlation
'" between genotype and phenotype. *Br J Dermatol* , 1365-9.
(" (2011).
)" Expanding the keratin mutation database: novel and recurrent mutations and genotype-phenotype
*" correlations in 28 patients with epidermolytic ichthyosis. *Br J Dermatol* , 442-7.
!+" (2010). An update on the genetics of atopic dermatitis: scratching the surface in
!!" 2009. *J Allergy Clin Immunol* , 16-29 e1-11; quiz 30-1.
!#"
!$" (2012). Expression signature of epidermolysis bullosa simplex.
!%" *Hum Genet* , 393-406.
!&" (2012). One remarkable molecule: filaggrin. *J Invest*
!'" *Dermatol* , 751-62.
!(" (2005). The cornified envelope: a model of cell death in
!)" the skin. *Nat Rev Mol Cell Biol* , 328-40.
!*"
#+" (1998). A highly conserved lysine residue on the head domain of type II keratins is
#!" essential for the attachment of keratin intermediate filaments to the cornified cell envelope through
##" isopeptide crosslinking by transglutaminases. *Proc Natl Acad Sci U S A* , 2067-72.
#$"
#%" (2011). Keratin gene mutations in disorders of human skin and its appendages. *Arch Biochem*
#&" *Biophys* , 123-37.
#'" (2011). The inflammasome NLRs in immunity,
#(" inflammation, and associated diseases. *Annu Rev Immunol* , 707-35.
#)" (2010). Keratin 17 promotes
#*" epithelial proliferation and tumor growth by polarizing the immune response in skin. *Nat Genet* , 910-4.
$+" (2009). Immunological and inflammatory functions of the interleukin-1 family.
$!" *Annu Rev Immunol* , 519-50.
$#" (2004). S100
$$" proteins in the epidermis. *J Invest Dermatol* , 23-33.
$%" (2009). The endogenous
$&" Toll-like receptor 4 agonist S100A8/S100A9 (calprotectin) as innate amplifier of infection,
$'" autoimmunity, and cancer. *J Leukoc Biol* , 557-66.
$(" (2007). The
$)" inflammasome mediates UVB-induced activation and secretion of interleukin-1beta by keratinocytes.
$*" *Curr Biol* , 1140-5.
%+" (2010). Interleukin-1,
%!" inflammasomes and the skin. *Eur J Cell Biol* , 638-44.
%#"
%$" (2010). Assessment of the psoriatic transcriptome in a large
%%" sample: additional regulated genes and comparisons with in vitro models. *J Invest Dermatol* , 1829-40.
%&"
%'" (2009). Global gene expression analysis reveals evidence for
%(" decreased lipid biosynthesis and increased innate immunity in uninvolved psoriatic skin. *J Invest*
%)" *Dermatol* , 2795-804.

(2009). Interleukin-33 - cytokine of dual function or novel alarmin? *Trends Immunol* , 227-33.

(2000). Role of interleukin-18 (IL-18) during lethal shock: decreased lipopolysaccharide sensitivity but normal superantigen reaction in IL-18-deficient mice. *Infect Immun* , 3502-8.

(2010). The inflammasome, an innate immunity guardian, participates in skin urticarial reactions and contact hypersensitivity. *Allergol Int* , 105-13.

(2012). Altered stratum corneum barrier and enhanced percutaneous immune responses in filaggrin-null mice. *J Allergy Clin Immunol* , 1538-46 e6.

(2008). GeneTrailExpress: a web-based pipeline for the statistical evaluation of microarray experiments. *BMC Bioinformatics* , 552.

(2012). Filaggrin loss-of-function mutations are associated with enhanced expression of IL-1 cytokines in the stratum corneum of patients with atopic dermatitis and in a murine model of filaggrin deficiency. *J Allergy Clin Immunol* , 1031-9 e1.

(2007). Intermediate filament scaffolds fulfill mechanical, organizational, and signaling functions in the cytoplasm. *Genes Dev* , 1581-97.

(2002). IL-18 contributes to the spontaneous development of atopic dermatitis-like inflammatory skin lesion independently of IgE/stat6 under specific pathogen-free conditions. *Proc Natl Acad Sci U S A* , 11340-5.

(2012). Association of serum interleukin-18 and other biomarkers with disease severity in adults with atopic dermatitis. *Arch Dermatol Res* , 305-12.

(2012). Epidermal barrier dysfunction and cutaneous sensitization in atopic diseases. *J Clin Invest* , 440-7.

(2004). Keratins and skin disorders. *J Pathol* , 355-66.

(2010). The ubiquitin ligase CHIP/STUB1 targets mutant keratins for degradation. *Hum Mutat* , 466-76.

(2004). Pathogenesis of human papillomaviruses in differentiating epithelia. *Microbiol Mol Biol Rev* , 362-72.

(2007). Induction of inflammatory cytokines by a keratin mutation and their repression by a small molecule in a mouse model for EBS. *J Invest Dermatol* , 2781-9.

(2007). Structural and regulatory functions of keratins. *Exp Cell Res* , 2021-32.

(2003). Loss of S100A9 (MRP14) results in reduced interleukin-8-induced CD11b surface expression, a polarized microfilament system, and diminished responsiveness to chemoattractants in vitro. *Mol Cell Biol* , 1034-43.

(2002). Keratin 17 null mice exhibit age- and strain-dependent alopecia. *Genes Dev* , 1412-22.

(2010). Enrichment map: a network-based method for gene-set enrichment visualization and interpretation. *PLoS One* , e13984.

(2009). Skin immune sentinels in health and disease. *Nat Rev Immunol* , 679-91.

(2010). Revised nomenclature and classification of inherited ichthyoses: results of the First Ichthyosis Consensus Conference in Soreze 2009. *J Am Acad Dermatol* , 607-41.

(2009). Genetic architecture of mouse skin inflammation and tumour susceptibility. *Nature* , 505-8.

(2001). Formation of a normal epidermis supported by increased stability of keratins 5 and 14 in keratin 10 null mice. *Mol Biol Cell* , 1557-68.

(2002). Hyperproliferation, induction of c-Myc and 14-3-3sigma, but no cell fragility in keratin-10-null mice. *J Cell Sci* , 2639-50.

(2009). Cytokines as genetic modifiers in K5-/- mice and in human epidermolysis bullosa simplex. *Hum Mutat* , 832-41.

(2008). Global expression profiling in atopic eczema reveals reciprocal expression of inflammatory and lipid genes. *PLoS One* , e4017.

(2001). Pathogenesis of the permeability barrier abnormality in epidermolytic hyperkeratosis. *J Invest Dermatol* , 837-47.

(2010). The inflammasomes. *Cell* , 821-32.

(2006). New consensus nomenclature for mammalian keratins. *J Cell Biol* , 169-74.

(2006). Epidermal barrier formation and recovery in skin disorders. *J Clin Invest* , 1150-8.

(1999). Klf4 is a transcription factor required for establishing the barrier function of the skin. *Nat Genet* , 356-60.

(2012). Keratins Mediate Localization of Hemidesmosomes and Repress Cell Motility. *J Invest Dermatol*.

(2011). Deconstructing the skin: cytoarchitectural determinants of epidermal morphogenesis. *Nat Rev Mol Cell Biol* , 565-80.

(2012). Inflammasomes in health and disease. *Nature* , 278-86.

(2010). Evaluation of the psoriasis transcriptome across different studies by gene set enrichment analysis (GSEA). *PLoS One* , e10247.

(2011). Nonlesional atopic dermatitis skin is characterized by broad terminal differentiation defects and variable immune abnormalities. *J Allergy Clin Immunol* , 954-64 e1-4.

(2012). Cytokeratins mediate epithelial innate defense through their antimicrobial properties. *J Clin Invest*.

(2006). Keratin 17 modulates hair follicle cycling in a TNFalpha-dependent fashion. *Genes Dev* , 1353-64.

(2009). Keratins regulate protein biosynthesis through localization of GLUT1 and -3 upstream of AMP kinase and Raptor. *J Cell Biol* , 175-84.

!"
#" (2007). Mrp8 and Mrp14 are endogenous activators of
$" Toll-like receptor 4, promoting lethal, endotoxin-induced shock. *Nat Med* , 1042-9.
%" (2012). Deletion of K1/K10 does not
&" impair epidermal stratification but affects desmosomal structure and nuclear integrity. *J Cell Sci* ,
'" 1750-8.
(" (2009). IL-18 and skin inflammation. *Autoimmun*
)" *Rev* , 45-8.
*" (2010). Sensing the outside world: TSLP regulates barrier immunity.
!+" *Nat Immunol* , 289-93.

!!" "

!#"

Krt1

( ) Hematoxylin/eosin-stained full-thickness back skin sections from *Krt1*$^{+/+}$ and *Krt1*$^{Đ/Đ}$ pups at P0. Scale bars: top, 20 µm; bottom, 10 µm. (and) Immunoblot analysis of Krt1 ( ) and Krt10 ( ) expression in total skin extracts from *Krt1*$^{+/+}$ and *Krt1*$^{Đ/Đ}$ pups at P0. Equal loading was assessed by Ponceau S staining of the blotted protein on nitrocellulose membranes ( ) or Coomassie staining of SDS-polyacrylamide gels run in parallel ( ). Molecular weight standards are indicated in kDa. ( ) Immunofluorescence staining of full-thickness back skin sections from *Krt1*$^{+/+}$ and *Krt1*$^{Đ/Đ}$ pups at P0 with antibodies against Krt1 and Krt10. Solid line indicates basement membrane. Scale bars, 10 µm. ( ) Immunofluorescence staining of full-thickness back skin sections from *Krt1*$^{+/+}$ and *Krt1*$^{Đ/Đ}$ pups at P0 with antibodies against Krt6 and Krt16. Solid line indicates basement membrane. Scale bars, 10 µm.

Krt1

(and) Double immunofluorescence staining of full-thickness back skin sections from *Krt1*$^{+/+}$ and *Krt1*$^{-/-}$ pups at P0 with antibodies against Krt5 and Krt10 ( ) or against Krt6 and Krt10 ( ). Solid line indicates basement membrane. Lower panels a`, a`` ( ), b`, b`` ( ) show magnified segments as indicated in the upper panels.Note absence of Krt5 or Krt6 in Krt10 aggregates. Scale bars, 10 µm. (, and) Immunofluorescence staining offull-thickness back skin sections from *Krt1*$^{+/+}$ and *Krt1*$^{Đ/Đ}$ pups at P0 to visualize distribution ofdesmoplakin ( ), desmoglein ( ) and plakoglobin ( ). Solid line indicates basement membrane. Lower panels c`, c`` ( ), d`, d`` ( ) show magnified segments as indicated in the upper panels.Note unaltered colocalization and distribution of major desmosomal proteins in the absence of Krt1. Scale bars, 10 µm.

Krt1

( ) Toluidine blue dye exclusion assay of *Krt1*$^{+/+}$ and *Krt1*$^{Đ/Đ}$ pups at P0. ( )Gross morphology of CEs from *Krt1*$^{+/+}$ and *Krt1*$^{Đ/Đ}$ skin at P0 after sonification for 0 or 4 min. Scale bars, 100 µm.

( ) Gross morphology of CEs from *Krt10*$^{+/+}$ and *Krt10*$^{Đ/Đ}$ skin at P0. Scale bars, 100 µm. ( ) Box-whisker-plot of transepidermal water loss (TEWL) of *Krt1*$^{+/+}$ (n=38), *Krt1*$^{+/Đ}$ (n=83), and *Krt1*$^{Đ/Đ}$ (n=43) pups at P0. The median and the 5th and 95th percentile are shown. **P*<0.05. ( ) Quantitative analysis of intact versus fragile CEs at P0 from three mice per genotype. Shown are the percentages of intact CEs. Values are mean ± s.e.m. **P*<0.05. ( ) Immunoblot analysis of Cldn1, Cldn4 and Cldn5 expression in total skin extracts from *Krt1*$^{+/+}$ and *Krt1*$^{Đ/Đ}$ pups at P0. Equal loading was assessed by Ponceau S staining of the proteins blotted on nitrocellulose membranes (not shown). Molecular weight standards are indicated in kDa. Note unaltered amounts of claudins in both genotypes of mice.

Krt1

( ) Cluster analysis and heat maps of differentially expressed genes in *Krt1*$^{Đ/Đ}$ skin at E18.5 (and) and P0 (and) associated with CE formation (and) and linked to immune response pathways (and). Samples from three mice per genotype were analyzed. Red indicates genes upregulated in *Krt1*$^{Đ/Đ}$ versus *Krt1*$^{+/+}$ skin. ( ) Global comparison analyses performed between the *Krt1* data set and genome-wide transcriptional profiling data sets derived from AE, psoriasis and EBS patients and the data set from the *Krt5*-targeted EBS mouse model, respectively. Shown are the numbers of identical gene identifiers present in the intersection of respective comparison analyses. ( ) Interconnected network of common regulated pathways present in both *Krt1*$^{Đ/Đ}$*versus* AE skin based on gene set enrichment analyses (GSEA) using the MSigDB database. The top 100 enriched pathways with a p-value < 0.001 were used; shown is the resulting pathway network of fully connected gene sets (cliques) grouped according to functional clusters. Depicted gene sets of the clusters are numbered and corresponding pathway IDs are listed in (see for details) (Merico et al., 2010).

Krt1

(and) Immunohistochemistry of full-thickness back skin sections from *Krt1*$^{+/+}$ and *Krt1*$^{Đ/Đ}$ pups at P0 against IL-18 ( ) and S100A8, S100A9 ( ). Scale bars, 20 µm.( ) Immunofluorescence staining of blood vessels with PECAM antibodies in back-skin sections of *Krt1*$^{Đ/Đ}$ and *Krt1*$^{+/+}$ mice at P0. Solid line indicates basement membrane. Scale bars, 20 µm.( ) ELISA analysis of IL-18, IL-33, and S100A8/A9 in newborn serum (P0) and epidermal protein extracts. Values are mean ± s.d. of duplicate measurements of pooled sera (*Krt1*$^{+/+}$, n=28; *Krt*$^{Đ/Đ}$, n=28) and epidermal extracts (n=6). **P*<0.05. ( ) IL-18 ELISA of serum samples from*Krt1*$^{Đ/Đ}$ and *Krt1*$^{+/+}$ mice at P2 either treated with an anti-IL-18-blocking antibody or remained mock treated. Values are mean ± s.e.m. of duplicate or triplicate measurements of pooled sera (n=3Đ12 mice). **P*<0.05. ( ) Gross morphology of CEs from *Krt1*$^{+/+}$ and *Krt1*$^{Đ/Đ}$ skin at P2 after anti-IL-18 blocking antibody treatment. Scale bar, 100 µm. ( ) Quantitative analysis of intact versus fragile CEs at P2 after treatment with IL-18 blocking antibodies (*Krt1*$^{+/+}$ IgG1, n=3; *Krt1*$^{+/+}$ anti-IL-18, n=1; *Krt1*$^{Đ/Đ}$ anti-IL-18, n=3; *Krt1*$^{Đ/Đ}$ vehicle, n=1 due to early neonatal lethality of untreated *Krt1*$^{Đ/Đ}$ mice). Shown are the percentages of intact CEs. Values are mean ± s.e.m. **P*<0.05.

Krt1$^{-/-}$ *Il18*

( ) Distribution of 4-6 week old *Krt1*/*Il18* genotypes derived from intercrosses of *Krt1*$^{+/-}$/Il18$^{+/-}$ mice.Indicated is the number of animals (obtained survivors/expected survivors according to the Mendelian frequency) of the indicated genotype out of a total of 255 4-6 week old offspring. 37 % of *Krt1*$^{+/-}$/Il18$^{+/-}$offspringsurvived. ( ) Hematoxylin/eosin-stained full-thickness back skin sections from *Krt1*$^{+/+}$, *Krt1*$^{Đ/Đ}$, *Krt1*$^{+/+}$*Il18*$^{Đ/Đ}$, *Krt1*$^{Đ/Đ}$*Il18*$^{Đ/Đ}$, *Krt1*$^{+/+}$*S100A9*$^{Đ/Đ}$, and *Krt1*$^{Đ/Đ}$*S100A9*$^{Đ/Đ}$ pups at P0. Scale bars, 20 µm. ( ) Immunofluorescence staining of full-thickness back skin sections from *Krt1*$^{+/+}$, *Krt1*$^{Đ/Đ}$, *Krt1*$^{+/+}$*Il18*$^{Đ/Đ}$,and *Krt1*$^{Đ/Đ}$*Il18*$^{Đ/Đ}$ pups at P0 with antibodies against Krt1 and Krt10. Solid line indicates basement membrane. Scale bars, 10 µm. ( ) Gross morphology of CEs from *Krt1*$^{+/+}$, *Krt1*$^{Đ/Đ}$, *Krt1*$^{+/+}$*Il18*$^{Đ/Đ}$, *Krt1*$^{Đ/Đ}$*Il18*$^{Đ/Đ}$, *Krt1*$^{+/+}$*S100A9*$^{Đ/Đ}$, and *Krt1*$^{Đ/Đ}$*S100A9*$^{Đ/Đ}$ skin at P0. Low differential interference contrast CEs were visualized using an artwork filter in Adobe Illustrator CS5.1. Scale bar, 100 µm. ( ) Quantitative analysis of intact *versus* fragile CEs at P0 from three mice per indicated genotype. Shown are the percentages of intact CEs. Values are mean ± s.e.m. **P*<0.05.

KRT1

( ) UVB irradiation of primary human keratinocytes mediates IL-18 secretion. Immunoblot analysis of cell culture supernatants (acetone concentrated) from primary human keratinocytes irradiated with 50 mJ/cm^2 or mock-treated in the presence or absence of the caspase-1 inhibitor YVAD (20 μM) or the pan-caspase inhibitor VAD (10 μM). ( ) Immunoblot analysis of IL-18, caspase-1 (CASP-1), and KRT1 in cell extracts and tissue culture supernatants concentrated by acetone precipitation from differentiated primary human keratinocytes after siRNA knockdown of *Krt1* (siKrt1)and casapse-1 (siCasp1). Scr, scrambled siRNA control. ( ) Immunofluorescence staining of wild-type and keratin cytoskeleton-free primary murine keratinocytes against NLRP3. Scale bars, 10 μm.

Data are compiled from knockout mice for Krt1 (this manuscript); Krt10 (Reichelt et al., 2001), Krt1/Krt10 (Wallace et al., 2012), Krt 17 (McGowan et al., 2002; Tong and Coulombe, 2006)."

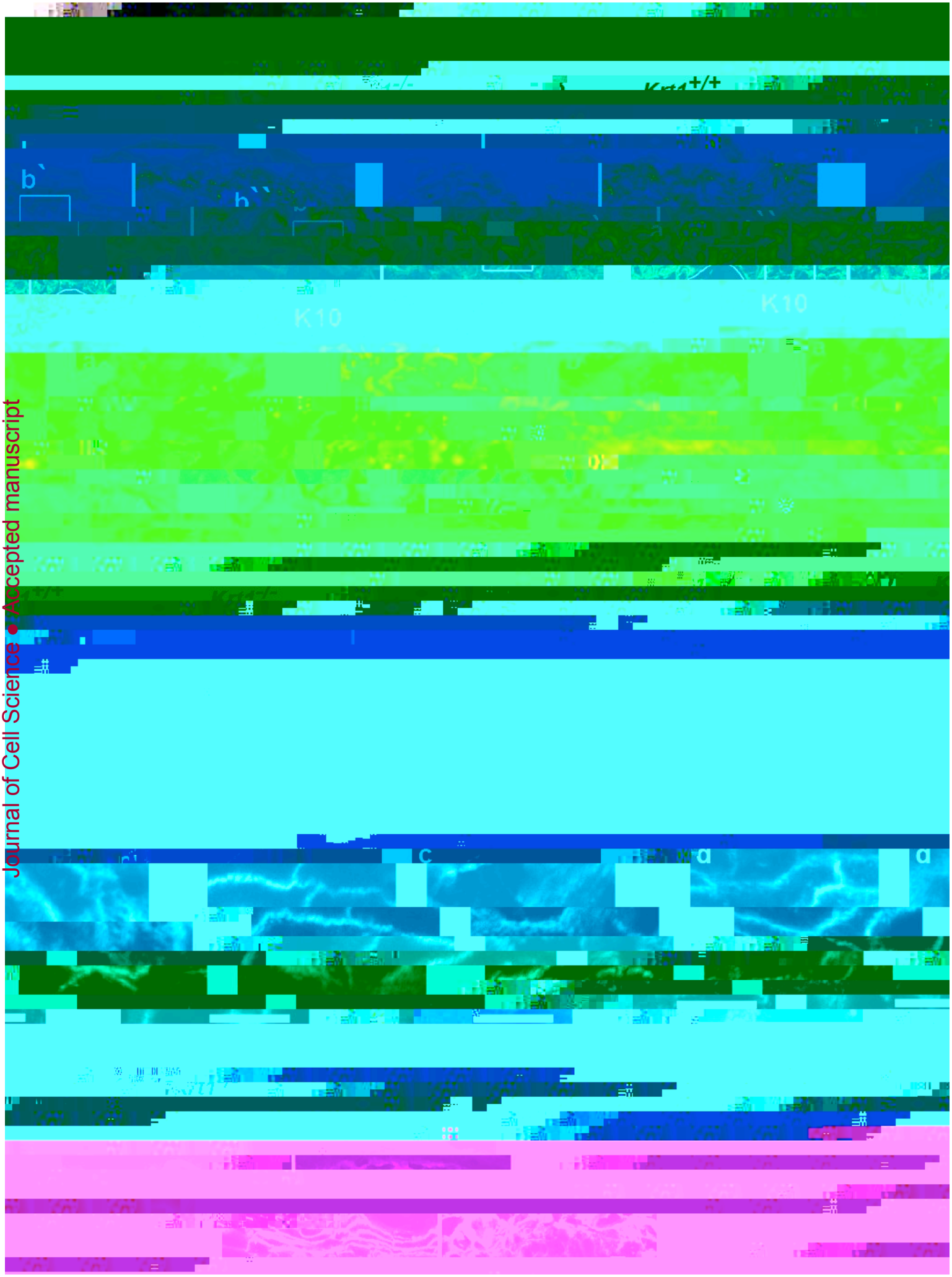

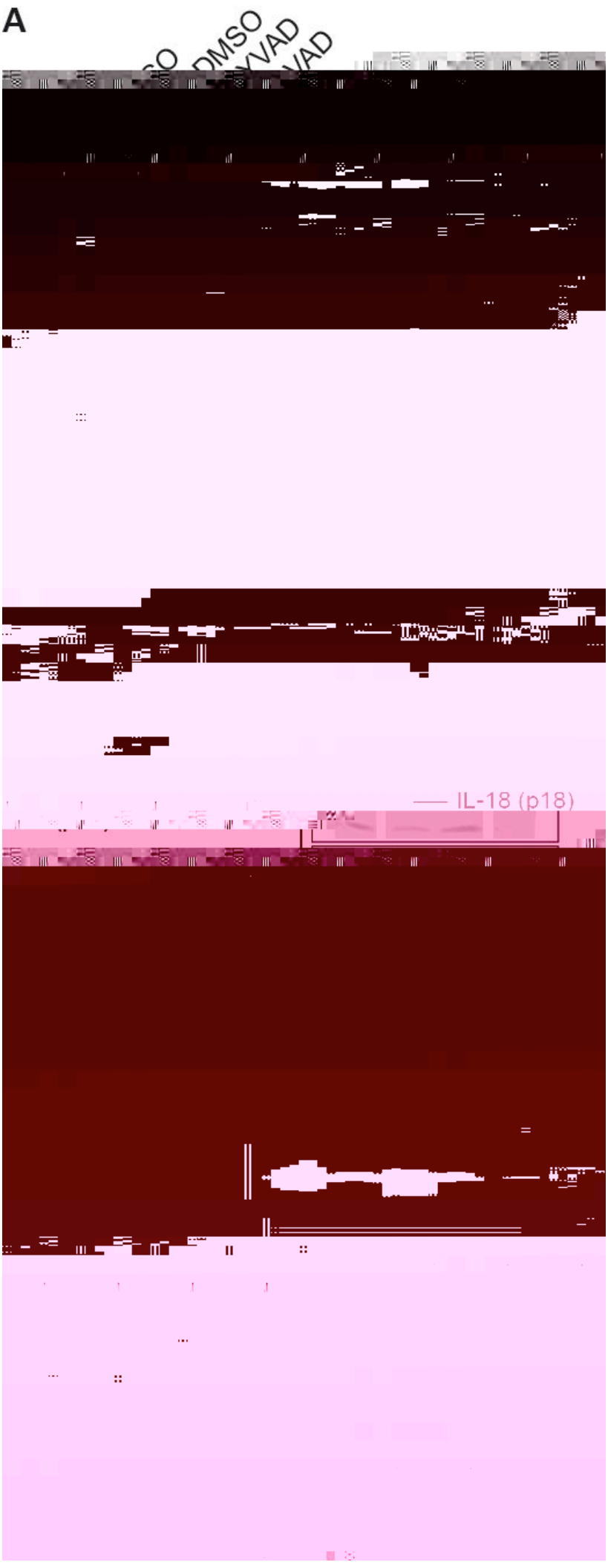

Roth_Fig 8

s r t on				
or p not p	In t on s n r t	H p r r tos s	r s n r t	A op n t on
t t		on		on
Ep r		non	s r	
H p r r tos s	r	stron	r	
TNFα p nt op				
H r s t no s				
E	2x↑	n t	ot on	ot on
Corn n op	nt t	nt t	nt t	ot on
In o u r n	n t		u	ot on
or r n	n t		u	ot on
F r n	n t	n t	n t	ot on
p t n	E t	ot on	ot on	ot on
ro r t on	n t	n t	n t	ot on
Co p ns tor r t n pr				